[28] Haas, R. A. and Guckel, G., "Stability of Electric Discharges in Flowing Molecular Gases," *Bulletin of the American Physical Society*, Vol. 16, No. 11, Nov. 1971, p. 1283.

[29] Hill, A. E., "Uniform Electrical Excitation of Large-Volume High-Pressure Near-Sonic CO_2–N_2–He Flowstream," *Applied Physics Letters*, Vol. 18, No. 5, March 1971, pp. 194–197.

APRIL 1972 AIAA JOURNAL VOL. 10, NO. 4

Analysis of an Electric Discharge CO_2 Mixing Laser

H. A. HASSAN* AND J. W. BORDEAUX†
North Carolina State University, Raleigh, N.C.

A one-dimensional model of an electric discharge CO_2 mixing laser is presented. The model takes into consideration chemical, vibrational, and thermal nonequilibrium effects. Starting from the entrance of the glow discharge duct, the conservation equations for the various constituents are integrated through the glow discharge and mixing regions. The effects of pressure, mass flow rates of the various species, and current density are discussed in detail. It is shown that, for given pressure and temperature at the entrance, the gain coefficient and power output increase with an increase in CO_2 flow rate; also, there is a current density, a He flow rate and an N_2 flow rate at which the gain coefficient is constant.

Introduction

RECENT interest in high-flow electric discharge CO_2 laser systems results from their continuous high-power capabilities and high efficiencies. Although the inversion mechanism in CO_2 molecules is well understood, there is a need to formulate a self-consistent model which takes into consideration the chemical, vibrational, and thermal nonequilibrium effects and thus serves as a basis for optimizing the laser parameters of interest.

The problem considered here is that of the electric discharge mixing laser system shown in Fig. 1. In this system, N_2 and He are premixed in an upstream stagnation chamber and the mixture is excited by a rectangular glow discharge. The CO_2 is injected downstream of the anode and upstream of the optical axis.

The model presented here treats molecules in different quantum states as different species and employs the conservation of species equations, the over-all momentum and energy equations, and an electron energy equation to describe the laser system. A survey of the various relaxation processes involving heavy particles and available rates was given in Ref. 1. The important reactions indicated in Ref. 1, together with appropriate electron-heavy particle collisions serve as the basis of the kinetics in this work. Thus, the three-level approximation for the energy levels of CO_2 (Refs. 2 and 3) is not employed.

The one-dimensional approximation is employed; this implies that the laser is of the gas transport type. The resulting equations are integrated starting from the entrance of the glow discharge duct through the glow discharge and mixing regions. As a result of this integration, one can calculate, as a function of the distance, the gain coefficient, power output, number densities of the various levels, gas and electron temperatures, velocity, and pressure. The effects of pressure, mass flow rates of the various species, and current density on the gain coefficient and power output are discussed in detail.

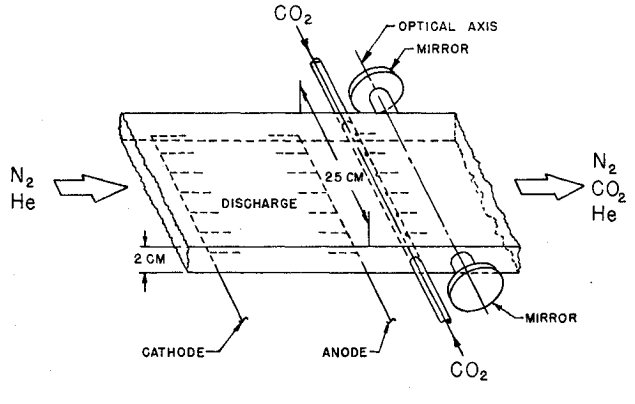

Fig. 1 Schematic of an electric discharge mixing laser.

Presented as Paper 71-66 at the AIAA 9th Aerospace Sciences Meeting, New York, January 25–27, 1971; submitted February 1, 1971; revision received September 29, 1971. Supported, in part, by NASA Grant NGR 34-002-115 and NSF Grant GY-7632.

Index categories: Lasers; Plasma Dynamics and MHD.

* Professor of Mechanical and Aerospace Engineering. Associate Fellow AIAA.

† Research Assistant.

Analysis

Treating molecules in different quantum states as different species, the governing equations are then the conservation of species equations, the over-all momentum and energy equations, and an electron energy equation.[4] The conservation of species equations can be written as

$$\partial\rho_i/\partial t + \nabla\cdot(\rho_i \boldsymbol{u}_i) = m_i R_i \equiv w_i \tag{1}$$

where, for species i, ρ_i is the density, m_i is the particle mass, $\boldsymbol{u}_i$ is the velocity, and R_i is the rate of production of species i. As a result of conservation of mass, summation of Eq. (1) with respect to i yields

$$\partial\rho/\partial t + \nabla\cdot(\rho\boldsymbol{u}) = 0 \tag{2}$$

where $\rho = \Sigma\,\rho_i$ is the mean density and $\boldsymbol{u} = (\Sigma\,\rho_i\boldsymbol{u}_i)/\rho$ is the mean velocity of the entire system. Letting

$$\boldsymbol{u}_i = \boldsymbol{u} + \boldsymbol{V}_i, \qquad Y_i = \rho_i/\rho \tag{3}$$

where $\boldsymbol{V}_i$ is the diffusion velocity, substituting into Eq. (1) and simplifying the resulting expression by using Eq. (2), one obtains

$$\rho(\partial Y_i/\partial t) + \rho\boldsymbol{u}\cdot\nabla Y_i + \nabla\cdot(Y_i\boldsymbol{V}_i) = w_i \tag{4}$$

The characteristic times of the various processes in a laser system can be obtained by writing Eq. (4) in dimensionless form. For the sake of this discussion, it will be assumed that the diffusion velocity is given by Fick's law.

$$V_i = -D_i \nabla \ln Y_i \tag{5}$$

where D_i is an appropriate diffusion coefficient. Letting L and d be typical length and diameter of a tube laser and u_o, ρ_o, D_o, and w_o be characteristic velocity, density, diffusion coefficient, and production rate, respectively, one finds, by writing Eq. (4) in dimensionless form, that the characteristic times are

$$t_o = L/u_o, \qquad t_d = d^2/D_o, \qquad t_r = \rho_o/w_o \tag{6}$$

The times t_o, t_d, and t_r are characteristic residence, diffusion, and relaxation times, respectively. When $t_d > t_o$, the laser is of the gas transport type; in this case the cooling is mainly convective. This can be seen from

$$t_d/t_o = d^2 u_o/D_o L = (4/\pi) L_e^{-1} (\dot{m} C_p/\lambda L), \quad L_e = \rho_o D_o C_p/\lambda \tag{7}$$

where L_e is the Lewis number (of order unity), $\dot{m}$ is the mass flow rate, C_p is the specific heat at constant pressure, and λ is the thermal conductivity. The parameter $\dot{m}C_p/\lambda L$ can be thought of as the ratio of the convective cooling to cooling by conduction and diffusion. Because t_d/t_o can be written in the alternative form

$$t_d/t_o = (d/L) ScRe, \qquad Sc = \mu/\rho_o D_o$$

where μ is the coefficient of shear viscosity, Sc is the Schmidt number and Re is the Reynolds number, the parameter $\dot{m}C_p/\lambda L$ is not a new dimensionless parameter.

To get an idea of the mass flow rates required for $t_d/t_o > 1$, values of C_p/λ representative of He at 450°K are employed. At this temperature

$$t_d/t_o \geq 1 \quad \text{if} \quad \dot{m}/L \geq 4 \times 10^{-4} \text{ g/sec cm} \tag{8}$$

It should be noted that when $t_d \gg t_o$ changes in the axial direction are more important than changes in the radial direction, and a one-dimensional model may be employed in describing the laser system.

In this work, a one-dimensional model is employed and the mass flow rate is chosen in accordance with Eq. (8). In this case, the conservation of species and over-all continuity equations for a steady-state laser reduce to

$$\rho u (dY_i/dx) = w_i \tag{9}$$

$$\rho u A = \dot{m} \tag{10}$$

where A is the cross-sectional area. The momentum equation is

$$\rho u (du/dx) + dp/dx = 0$$

For a constant area duct, it can be integrated directly; the result can be expressed as

$$(\dot{m}/A) u + p = P_o \tag{11}$$

where P_o is the stagnation pressure. In the glow discharge region, the over-all energy equation can be written as

$$\rho u \, d(h + u^2/2)/dx = jE - dq/dx \tag{12}$$

where

$$h = \sum \rho_s h_s/\rho \tag{13}$$

h_s is the specific enthalpy of species s, j is the current density, E is the electric field, and q is the heat loss per unit area and time. Downstream of the discharge region, Eq. (12) with $j = 0$ holds. The current density is related to the electric field by Ohm's law

$$j = \sigma_o E \tag{14}$$

where σ_o is the scaler electrical conductivity

$$\sigma_o = n_e e^2/m_e \nu_e, \qquad \nu_e = \sum_{e \neq s} \nu_{es} \tag{15}$$

and ν_{es} is the collision frequency between the electrons and species s. If subscripts 1, 2, 3 designate CO_2, N_2, and He, respectively, then the specific enthalpies can be written as

$$h_1 = \left[\frac{7}{2} + \sum_{i=1}^{4} \frac{\theta_i/T}{\exp(\theta_i/T) - 1}\right] \frac{k}{m_1} T + h_{o,1}$$

$$h_2 = \{\tfrac{7}{2} + (\theta/T)/[\exp(\theta/T) - 1]\}(k/m_2)T; \quad h_3 = \tfrac{5}{2}(k/m_3)T$$

where

$$\theta_i = 1932.1, 960.1, 960.1, 3380°\text{K}$$

$$\theta = 3353.9°\text{K} \tag{16}$$

and $h_{o,1}$ is the heat of formation of CO_2. The collision frequencies may be obtained from knowing ν_{et}/n_t, which is a function of the electron temperature, or from knowledge of the collision cross section Z_{st}, which is related to the collision frequency by the relation

$$\nu_{st} = \tfrac{2}{3}[2k(T_s/m_s + T_t/m_t)]^{1/2} n_t Z_{st} \tag{17}$$

In this work, Z_{et} for He, and ν_{et}/n_t for N_2 and CO_2 were obtained as functions of the electron temperature, from Refs. 5–7, respectively.

The electron temperature, collision frequencies and species conservation equations depend on the forms of the velocity distribution functions in the gas. The equations employed here can be derived from the appropriate Boltzmann equations by using the 13-moment method.[8] In this method, deviations of the distribution functions from uniformity and from Maxwellian distributions are assumed small. At low pressures and high-electric fields, departures from Maxwellian are not small and the distribution functions would have to be computed from the appropriate Boltzmann equations. Such calculations were carried out for slightly ionized uniform gases in Refs. 6, 7, 9, and 10. Because the solution of the Boltzmann equations, even in the absence of spatial nonuniformity, is a major undertaking, such procedure was not employed in this study; instead, it was decided to employ the multifluid equations and utilize available experimental data. In the few cases where needed data was not available from experiment, a Maxwellian distribution function was employed in conjunction with experimentally measured cross sections. It would have been desirable to use more realistic distribution functions, because of this, our approach raises some questions which can only be resolved by detailed comparison of theory and experiment. Further consideration of this point will be given when the results of the computations are discussed.

The quantity dq/dx is the sum of the wall losses and laser power output. The one-dimensional approximation implies that the wall losses are small and thus dq/dx reduces to the laser power output per unit volume

$$dq/dx = \gamma I \tag{18}$$

where γ is the gain coefficient and I is the radiation intensity. The expression for γ may be written as[3]

$$\gamma = (c^3/8\pi\nu^2) g_m A_{mn} (N_m/g_m - N_n/g_n) G \tag{19}$$

where $m, n (m > n)$, designate the two states between which transitions are allowed; N_m, N_n are the number densities; g_m, g_n are the degeneracies; A_{mn} is the Einstein coefficient of spontaneous emission; ν is the frequency; c is the speed of light; and G is the shape factor. If the power output is made to occur on a single P-branch transition of the $(0, 0^0, 1) - (1, 0^0, 0)$ band, usually $P(20)$ at 10.6 μ, then Eq. (19) can be cast in a different form. Letting n_s, n_t designate the number density of particles in the $(0, 0^0, 1)$ and $(1, 0^0, 0)$ vibrational levels, respectively, one finds[3]

$$N_m = (2hc/kT) B_s g_m n_s \exp[-hcB_s m(m+1)/kT], \quad m = 20$$

$$N_m = (2hc/kT) B_t g_n n_t \exp[-hcB_t n(n+1)/kT], \quad n = 19 \tag{20}$$

where

$$g_m = 2m + 1 \tag{21}$$

and B_s and B_t are the rotational constants of the $(0, 0^0, 1)$ and $(1, 0^0, 0)$ levels, respectively, which can be obtained from Ref. 11.

An expression for the shape factor G, which takes into consideration both homogeneous and Doppler broadening, can be written as[3]

$$G = (2/\pi^{1/2})(1/\Delta\nu_c)\delta \exp \delta^2 \operatorname{erfc} \delta \tag{22}$$

where

$$\delta = \Delta\nu_c(\ln 2)^{1/2}/\Delta\nu_D$$

$$\Delta\nu_c = \frac{1}{\pi\tau} = \frac{1}{\pi}\sum_t \nu_{st}, \qquad s = 1, \qquad t = 1, 2, 3 \tag{23}$$

$$\Delta\nu_D = 2(\nu/c)(2kT \ln 2/m_1)^{1/2}$$

$\Delta\nu_c$ is the homogeneous half-width and $\Delta\nu_D$ is the Doppler half-width. The collision frequencies ν_{st} are obtained from Eq. (17) and the cross sections Z_{st} are these appropriate for a Lennard-Jones (6–12) potential[12]

The last equation to be considered is the electron energy equation. After some manipulation, one obtains

$$\frac{5}{2}n_e u k\frac{dT_e}{dx} - u\frac{dP_e}{dx} = jE + n_e\sum 3\frac{m_e}{m_s}\delta_s\nu_{es}k(T_s - T_e) - \left(\frac{5kTe}{2} + 2\varepsilon\right)R_e \tag{24}$$

where subscript e designates electrons, ε is the ionization potential, and δ_s is the loss factor for species s, which is unity for monatomic gases. The quantity

$$3m_e\delta_s\nu_{es}/m_s n_s \equiv \nu_{us}/n_s \tag{25}$$

is a function of the electron temperature and was obtained for N_2 and CO_2 from Refs. 6 and 7, respectively.

Relaxation Processes in the Laser System

To complete the formulation of the problem one needs to identify the important relaxation processes and evaluate the production terms R_s. For an electric discharge CO_2 laser system the important reactions will be taken as

$$N_2 + e \rightleftarrows N_2^+ + e + e \tag{26a}$$

$$N_2(v = 0) + e \rightleftarrows N_2(v = 1) + e \tag{26b}$$

$$CO_2(0, 0^0, 1) \rightleftarrows CO_2(1, 0^0, 0) + h\nu \tag{26c}$$

$$CO_2(0, 1^1, 0) + M \rightleftarrows CO_2(0, 0^0, 0) + M + 667\ \text{cm}^{-1} \tag{26d}$$

$$CO_2(0, 0^0, 1) + N_2(v = 0) \rightleftarrows CO_2(0, 0^0, 0) + N_2(v = 1) + 18\ \text{cm}^{-1} \tag{26e}$$

$$CO_2(0, 0^0, 1) + M \rightleftarrows CO_2(0, 3^1, 0) + M + 416\ \text{cm}^{-1} \tag{26f}$$

where M stands for any species in the system: CO_2, N_2, He. In addition, it will be assumed that the bending and symmetric stretching modes are in equilibrium at some temperature T_v which was found to be not much different from T, the gas temperature. In writing the preceding reactions, it is assumed that CO, H_2O, and other impurities have little influence on the laser system. Recent measurements indicate that the fractional concentration of CO decreases with increasing velocity in CO_2 laser systems[13]; this may serve as a partial justification for neglecting CO in this analysis. For the sake of simplicity of notation, the number densities of $CO_2(0, 0^0, 0)$, $CO_2(0, 1^1, 0)$, $CO_2(0, 2^0, 0)$, $CO_2(0, 3^1, 0)$, $CO_2(1, 0^0, 0)$, $CO_2(0, 0^0, 1)$, $N_2(v = 0)$, $N_2(v = 1)$, N_2^+, He will be designated by $n_0, \ldots, n_9$, respectively.

Expressions for the rates of production R_i can now be written by utilizing the law of mass action[14] and Eq. (26). All reactions shown in Eq. (26) fit into the general category

$$\sum a_i A_i \underset{K_b}{\overset{K_f}{\rightleftarrows}} \sum b_i A_i \tag{27}$$

where K_f and K_b are the forward and backward rate constants and are usually functions of temperature. The contribution of the above reaction to the rate of production of species i is

$$(b_i - a_i)(K_f\Pi n_j^{aj} - K_b\Pi n_j^{bj}) \tag{28}$$

The quantities R_i are obtained by summing contributions of the type given by Eq. (28) for the various reactions that produce species i; their explicit expressions are given in the Appendix.

Data for computing the forward rates K_f are available for all the reactions indicated in Eq. (26) and the backward rates are determined from the principle of detailed balancing.[14] Thus, plots of the K_f's for reactions (26d–f) are given as functions of temperature in Ref. 1 and the rate for reaction (26c) follows directly from Eqs. (18) and (19). On the other hand, cross sections for computing the K_f's for reactions (26a) and (26b) are given in Refs. 15 and 16, respectively. The following expression may be used to compute K_f in terms of the cross section Q

$$K_f = \left(\frac{8}{\pi m_e}\right)^{1/2}\frac{1}{(kT_e)^{3/2}}\int_\varepsilon^\infty \exp\left(-\frac{\eta}{kT_e}\right)\eta Q(\eta)d\eta \tag{29}$$

where ε is the ionization or excitation energy and Q is the appropriate cross section. Following the suggestion of Ref. 17, an effective cross section, which is the total cross section for vibrational excitation up to the eighth level is employed for reaction (26b); the total cross section at the peak was taken as 3.8×10^{-16} cm^2.

Before one can compute the small signal gain and power output, one needs to specify or provide an additional relation to calculate the intensity. For the gain coefficient calculation, a small value of the intensity is assumed; the value employed here is that given by Planck's function. On the other hand, when computing the laser power output an additional relation is needed to determine the intensity and this relation is provided by the threshold condition. If y is the direction of the optical axis and l is the distance between the mirrors, then the threshold condition can be written as[3]

$$\frac{1}{l}\int_0^l \gamma\, dy = -\frac{\ln(r_1 r_2)}{2l} \tag{30}$$

where r_1 and r_2 are the reflectivity of the mirrors. When Eq. (30) is used in conjunction with the governing equations, the intensity is calculated as part of the solution and this, in turn, gives the laser power output P as[3]

$$P = A\int_0^w \gamma I\, dx \tag{31}$$

where w is the width of the mirrors. In writing Eq. (31) it was assumed that mirror losses are negligible.

Results and Discussion

The schematic shown in Fig. 1 is that of a device which is being built at the NASA Langley Research Center to study electric discharge mixing lasers. The device is not in operation yet and, therefore, we have no way of comparing the predictions of this theory with experiment. When carrying out the computations, one needs to specify, in addition to the dimensions of the device, the current density, the mass flow rates of N_2, CO_2, and He and the conditions at the entrance of the glow discharge duct, $x = 0$; this entails specifying the pressure, gas temperature, electric field, and concentrations of the heavy species. The electron temperature and concentration at $x = 0$ are obtained from Ohm's law and a simplified energy equation, which is Eq. (24) without the gradient terms. Unless indicated otherwise, the results shown in Figs. 2–11 are for $\dot{m}_1 = 0.9$ g/sec, $\dot{m}_2 = 1.8$ g/sec, $\dot{m}_3 = 0.9$ g/sec, $p_o = 20$ torr, $T_o = 300$°K, $j = 25$ ma/cm^2, $r_1 r_2 = 0.76$; subscripts 1, 2, 3 designate CO_2, N_2, and He, respectively, while subscript o indicates conditions at $x = 0$; $\xi = x/L$, $L = 50$ cm.

The electric field and the concentrations of the heavy particles are not well known at $x = 0$. Values of E_o ranging from 300 v/cm

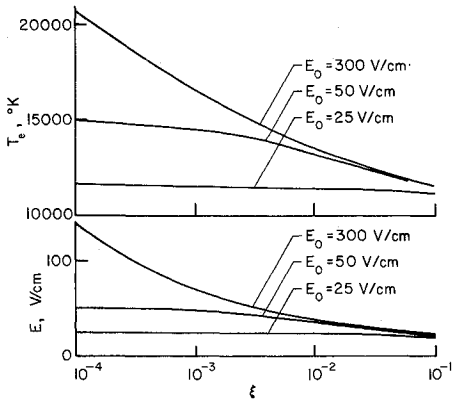

Fig. 2 Electric field and electron temperature vs distance.

to 25 v/cm were employed and the initial concentrations were obtained assuming equilibrium at the gas temperature and pressure. As is seen from Fig. 2, the electric field levels off quickly to a value of the order of 25 v/cm independent of E_o. The low value of the electric field can be traced to the assumption of Maxwellian distribution in Eq. (29). Non-Maxwellian velocity distributions of the type shown in Refs. 6 and 10 will yield lower ionization rates, this will result in a smaller number density for the electrons and thus higher electric fields for a given current density. It was also found that the concentrations of the various species were not sensitive to the initial choice of the electric field and concentrations. Because T_e is proportional to $jE = \sigma_o E^2$, the electron temperature will have a behavior similar to that of the electric field, as shown in Fig. 2.

Because the pressure and temperatures in the glow discharge region are practically constant, the various rates of production are proportional to the concentrations and any overestimate or underestimate of the initial concentration of any species will quickly adjust to values dictated by the rates. Moreover, the concentrations have the tendency to "freeze" at a certain value; freezing is characterized by small derivatives of Y_s. A typical illustration of this phenomenon is shown in Fig. 3, which shows

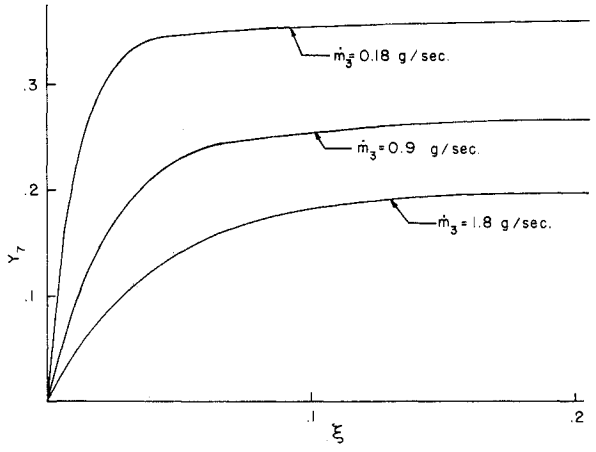

Fig. 3 Influence of He flow rate on excited N_2.

a plot of Y_7, the mass fraction of excited nitrogen, vs ξ in the glow discharge region. This freezing is responsible for the behavior of the electric field at constant current: as can be seen from Ohm's law, when the electron density is practically constant, the electric field will behave in a similar manner.

The effects of the pressure, mass flow rates of the various constituents, and current density on the gain coefficient are discussed next. The following results are based on the assumption that mixing CO_2 with N_2 and He is instantaneous at the point of injection. For a given mass flow rate, the velocity increases when the pressure decreases. Also, for the assumed entrance temperature, which is taken as 300°K for all the cases discussed here, increasing the pressure will result in an increase in the number densities. The influence of the entrance pressure on the gain is shown in Fig. 4. At the lower pressures or high velocities, the gain remains fairly constant as a result of freezing of the upper and lower laser levels. On the other hand, at the higher pressures where the velocity is lower, the gain peaks and is followed by a steady decline. The peak results from a combination of high number densities and low velocities; the latter makes it possible for the reaction to be completed in a shorter distance from the injection region.

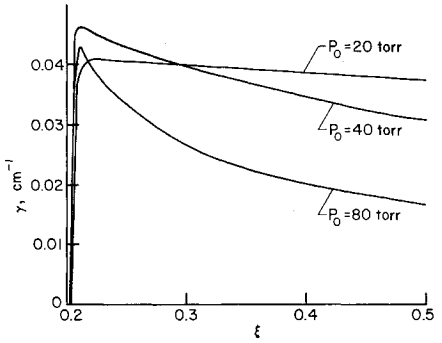

Fig. 4 Effect of entrance pressure on gain coefficient.

The effect of N_2 flow rate on the gain coefficient is discussed next. For a given initial pressure and temperature and He and CO_2 flow rates, increasing the mass flow of N_2 results in an increase in its partial pressure and this, in turn, implies an increase in n_7. On the other hand, increasing the mass flow rate at a given pressure results in an increase in velocity. Thus, there is an N_2 flow rate at a given pressure and temperature which results in an optimum gain in the region immediately downstream of the injection point. The effect of velocity becomes small further downstream and the gain will increase with the mass flow rate. This behavior is indicated in Fig. 5. Figure 6 shows that the gain coefficient increases with an increase in the mass flow rate of CO_2 for given N_2 and He flow rates; this is a result of the increase in the number of particles in the upper laser level.

The effect of He flow rate on the gain coefficient for given N_2 and CO_2 flow rates and entrance pressure and temperature is

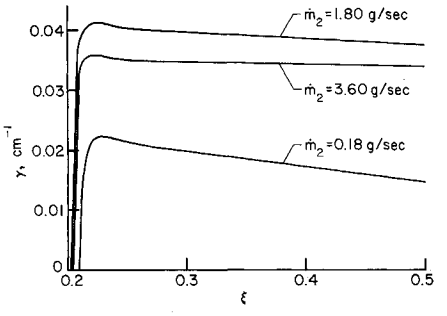

Fig. 5 Effect of N_2 flow rate on gain coefficient.

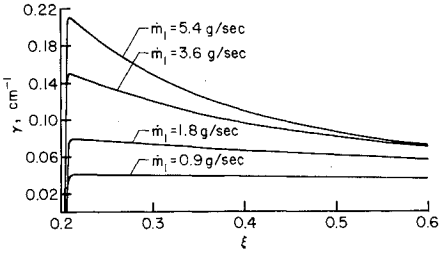

Fig. 6 Influence of CO_2 flow rate on gain coefficient.

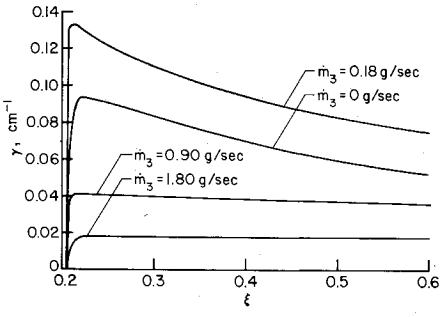

Fig. 7 Influence of He flow rate on gain coefficient.

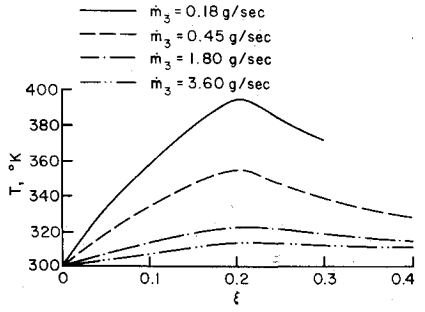

Fig. 8 Temperature distribution for various He flow rates.

shown in Fig. 7. Increasing the He mass flow rate at given entrance pressure and temperature results in an increase in velocity, a decrease in the partial pressure of N_2 and gas temperature, and an increase in the electron temperature. Because the rate of production of n_7 increases with T_e (up to $T_e \simeq 2$ ev) and the number density of N_2, one would expect that there is a mass flow rate at which n_7 is maximum. This and the rise in temperature at the low He flow rates indicated in Fig. 8 is responsible for the behavior shown in Fig. 7.

Available measurements[18] indicate that 4% is typical of the peaks of small signal gain coefficients. Except for values at the high CO_2 flow rates, and low He flow rates which at fixed initial pressure result in an increase in CO_2 or N_2 flow rates, the gain coefficient calculated here is typical of measured values. The reason for the discrepancy at the high CO_2 flow rates can be traced to the assumption of instantaneous mixing, and the abundance of excited N_2. The abundance of excited N_2 can result from any of the following assumptions made in this work. The use of a Maxwellian distribution in Eq. (29) overestimates the number of electrons and the rate constant for the production of excited nitrogen. However, the recent calculation of Ref. 19 show that the gain coefficient is insensitive to the type of distribution function employed in calculating the excitation rate of N_2. Also, using the suggestion of Ref. 17 regarding the cross section of N_2 excitation and, neglecting the effects of impurities, such as H_2O, which are effective in de-exciting both the excited N_2 and the upper laser level, will result in an overestimate of excited N_2. Additional calculations and careful measurements are needed to clarify this point.

Finally, the effect of current density on gain is discussed. As is seen from Fig. 9, the gain coefficient increases and then decreases with current density in the region immediately downstream of the injection point. Increasing the current density will result in an increase in the electron density and gas temperature. In the discharge region this will have the effect of increasing n_7, which will result in an increase in the gain coefficient. Conversely, an increase in temperature will result in an increase in the population density of the lower laser level; in addition, the increase in temperature at a given pressure will result in a decrease in the number density of CO_2 and this will decrease the gain coefficient. Thus, there is a current density at which the gain is optimum.

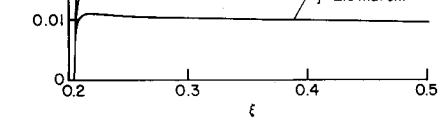

Fig. 9 Effect of current density on gain coefficient.

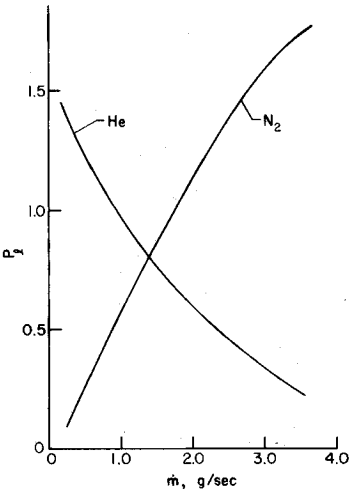

Fig. 10 Influence of He and N_2 flow rates on laser power output (dimensionless).

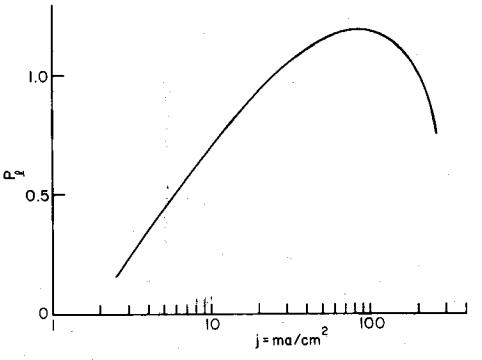

Fig. 11 Effect of current density on laser power output (dimensionless).

Figures 10 and 11 show a plot of P_l, the laser power output normalized with respect to the laser power output at $\dot{m}_1 = \dot{m}_3 = 0.9$ g/sec, $\dot{m}_2 = 1.8$ g/sec, and $j = 25$ ma/cm^2. For the range of parameters considered here, it is found that P_l increases with CO_2 (not shown) and N_2 flow rates and decreases with He flow rate. In addition, there is a current density at which the power output is maximum. The interpretation of the results shown in Figs. 10 and 11 follows closely the discussion of Figs. 5–9.

Conclusions

Except for the high CO_2 flow rates, the trends predicted by this theory are in good agreement with available measurements on electric discharge mixing and convective lasers.[18,19] This suggests

that the model employed here is basically sound. It is believed that the difficulty at higher CO_2 flow rates can be removed if one relaxes the assumption of instantaneous mixing, employs non-Maxwellian distribution functions when calculating excitation and ionization rates, and includes the effect of impurities.

Appendix: Explicit Expressions for the Production Rates

From charge neutrality and reaction (Eq. 26a), one obtains

$$R_8 = K_{1,f} n_6 n_e - K_{1,b} n_8 n_e^2, \qquad n_8 = n_e \tag{A1}$$

Using the principle of detailed balancing, one obtains at equilibrium

$$K_{1,f} n_6 n_e = K_{1,b} n_8 n_e^2$$

or,[4]

$$\frac{n_8 n_e}{n_6} = \frac{K_{1,f}}{K_{1,b}} = 2\frac{g_i}{g_a}\left(\frac{2\pi m_e k T_e}{h^2}\right)^{3/2} \exp\frac{-\varepsilon}{kT_e} \tag{A2}$$

with $g_i/g_a = 2$ for N_2. From reactions (26b) and (26e),

$$R_7 = K_{2,f} n_6 n_e - K_{2,b} n_7 n_e + K_{5,f} n_5 n_6 - K_{5,b} n_o n_7 \tag{A3}$$

where

$$K_{2,b} = K_{2,f} \exp(hc\omega/kT_e), \qquad \omega = 2331\ \text{cm}^{-1}$$

and

$$K_{5,b} = K_{5,f} \exp(-hc\omega/kT), \qquad \omega = 18\ \text{cm}^{-1} \tag{A4}$$

The rate of production of n_6 follows from reactions (26a), (26b), and (26d), or from the conservation of element equation, which can be written as

$$\dot{m}_2 = m_2(n_6 + n_7 + n_8)uA \tag{A5}$$

where $\dot{m}_2$ is the mass flow rate of N_2.

From reactions (26c), (26e), and (26f) and Eq. (18)

$$R_5 = -\gamma I/h\nu - K_{5,f} n_5 n_6 + K_{5,b} n_o n_7 - K_{6,f,1} n_5 n_o + K_{6,b,1} n_3 n_o - K_{6,f,2} n_5 n_6 + K_{6,b,2} n_3 n_6 \tag{A6}$$

where $K_{6,f,j}$ $(j = 1, 2, 3)$ are the forward rate constants for reaction (26f), with $j = 1, 2, 3$ designating CO_2, N_2, and He, respectively, while $K_{6,b,j}$ are the corresponding backward rate constants and are given by

$$K_{6,b,j} = K_{6,f,j} \exp(-hc\omega/kT), \qquad \omega = 416\ \text{cm}^{-1} \tag{A7}$$

The rate of production of n_3 follows from reaction (26f) as

$$R_3 = K_{6,f,1} n_5 n_o - K_{6,b,1} n_3 n_o + K_{6,f,2} n_5 n_6 - K_{6,b,2} n_3 n_o \tag{A8}$$

Similarly, from reaction (26d), one has

$$R_1 = -K_{4,f,1} n_1 n_o + K_{4,b,1} n_o^2 - K_{4,f,2} n_1 n_6 + K_{4,b,2} n_o n_6 - K_{4,f,3} n_1 n_9 + K_{4,b,3} n_o n_9 \tag{A9}$$

with

$$K_{4,b,j} = K_{4,f,j} \exp(-hc\omega/kT), \qquad \omega = 667\ \text{cm}^{-1} \tag{A10}$$

It will be assumed at this stage that all bending and symmetric stretching modes are in equilibrium at some temperature T_v, which is defined by the relation

$$n_3/n_1 = 2 \exp[-(hc/kT_v)(\omega_2 - \omega_1)] \tag{A11}$$

where $\omega_3 = 1932.5\ \text{cm}^{-1}$ and $\omega_1 = 667.3\ \text{cm}^{-1}$. With T_v defined by the above equation, one has

$$n_2/n_1 = \tfrac{3}{2} \exp[-(hc/kT_v)(\omega_2 - \omega_2)] \tag{A12}$$

$$n_4/n_1 = \tfrac{1}{2} \exp[-(hc/kT_v)(\omega_4 - \omega_1)] \tag{A13}$$

with $\omega_2 = 1285.5\ \text{cm}^{-1}$ and $\omega_4 = 1388.3\ \text{cm}^{-1}$. Formulas (A11–A13) assume a harmonic oscillator model and are appropriate for a symmetric linear molecule with a doubly degenerate bending mode. It should be noted that, in practice, a CO_2 molecule in equilibrium does not follow a harmonic oscillator model; this is why $\omega_2 \neq 2\omega_1$ and $\omega_3 \neq 3\omega_1$. To calculate n_o, one can write the appropriate rate equation or use the conservation of element principle.

References

[1] Taylor, R. L. and Bitterman, S., "Survey of Vibrational Relaxation Data for Processes Important in the CO_2–N_2 Laser System," *Reviews of Modern Physics*, Vol. 41, No. 1, Jan. 1969, pp. 26–47.

[2] Moore, C. B. et al., "Vibrational Energy Transfer in CO_2 Lasers," *The Journal of Chemical Physics*, Vol. 46, No. 11, June 1967, pp. 4222–4231.

[3] Cool, T. A., "Power and Gain Characteristics of High Speed Flow Lasers," *Journal of Applied Physics*, Vol. 40, No. 9, Aug. 1969, pp. 3563–3573.

[4] Sutton, G. W. and Sherman, A., *Engineering Magnetohydrodynamics*, 1st ed., McGraw-Hill, New York, 1965, pp. 111–123, 198–201, 225.

[5] Frost, L. S. and Phelps, A. V., "Momentum-Transfer Cross Sections for Slow Electrons in He, Ar, Kr, and Xe from Transfer Coefficients," *Physical Review*, Vol. 136, No. 6A, Dec. 1964, pp. A1538–A1545.

[6] Engelhardt, A. G. et al., "Determination of Momentum Transfer and Inelastic Collision Cross Sections for Electrons in Nitrogen Using Transport Coefficients," *Physical Review*, Vol. 135, No. 6A, Sept. 1964, pp. A1566–A1574.

[7] Hake, R. D. Jr. and Phelps, A. V., "Momentum-Transfer and Inelastic-Collision Cross Sections for Electrons in O_2, CO, and CO_2," *Physical Review*, Vol. 158, No. 1, June 1967, pp. 70–84.

[8] Burgers, J. M., *Flow Equations for Composite Gases*, 1st ed., Academic Press, New York, 1969, pp. 58–64.

[9] Frost, L. S. and Phelps, A. V., "Rotational Excitation and Momentum Transfer Cross Sections for Electrons in H_2 and N_2 from Transport Coefficients," *Physical Review*, Vol. 127, No. 5, Sept. 1962, pp. 1621–1633.

[10] Nighan, W. L., "Electron Energy Distributions and Collision Rates in Electrically Excited N_2, CO, and CO_2," *Physical Review A*, Vol. 2, No. 5, Nov. 1970, pp. 1989–2000.

[11] Herzberg, G., *Molecular Spectra and Molecular Structure, II. Infrared and Raman Spectra of Polyatomic Molecules*, 1st ed., Van Nostrand, New York, 1945, pp. 340–395.

[12] Hirschfelder, J. O., Curtiss, C. F., and Bird, R. B., *Molecular Theory of Gases and Liquids*, Wiley, New York, 1964, pp. 523–582.

[13] Wiegand, W. J. et al., "Carbon Monoxide Formation in CO_2 Lasers," *Applied Physics Letters*, Vol. 16, No. 6, March 1970, pp. 237–239.

[14] Williams, F. A., *Combustion Theory*, 1st ed., Addison-Wesley, Reading, Mass., 1965, pp. 358–361.

[15] Rapp, D. and Englander-Golden, P., "Total Cross Section for Ionization and Attachment in Gases by Electron Impact. I. Positive Ionization," *The Journal of Chemical Physics*, Vol. 43, No. 5, Sept. 1965, pp. 1464–1479.

[16] Schulz, G. J., "Vibrational Excitation of N_2, CO, and H_2 by Electron Impact," *Physical Review*, Vol. 135, No. 4A, Aug. 1964, pp. A988–A994.

[17] Sobolev, N. N. and Sokovikov, V. V., "Inversion Mechanisms in CO_2 High Intensity Gas Lasers," *The Physics of Electronic and Atomic Collisions*, edited by L. M. Branscomb, Univ. of Colorado Press, Boulder, 1968, pp. 49–60.

[18] Brown, C. O., "High-Power CO_2 Electric Discharge Mixing Laser," *Applied Physics Letters*, Vol. 17, No. 9, Nov. 1970, pp. 388–391.

[19] Seals, R. K. Jr. et al., "Theory and Experiment of Electric Discharge CO_2 Convection Lasers," AIAA Paper 71-588, 1971.